IEEE Access
Multidisciplinary | Rapid Review | Open Access Journal

Received January 20, 2020, accepted February 24, 2020, date of publication March 4, 2020, date of current version March 19, 2020.

Digital Object Identifier 10.1109/ACCESS.2020.2978258

Robust Integral Backstepping Control for Unified Model of Hybrid Electric Vehicles

SYED AHMAD SIFFAT, IFTIKHAR AHMAD, AQEEL UR RAHMAN, AND YASIR ISLAM
School of Electrical Engineering and Computer Science, National University of Sciences and Technology (NUST), Islamabad 44000, Pakistan
Corresponding author: Iftikhar Ahmad (iftikhar.rana@seecs.edu.pk)

ABSTRACT Exponential decrease in oil and natural gas resources, increasing global warming issues and insufficiency of fossil fuels has shifted the focus to fuel cell hybrid electric vehicles (FHEVs). FHEV model used in this work consists of fuel cell, ultracapacitor and battery. Non-linearities present in the vehicle model dominate because of extreme driving conditions like rough terrains, slippery roads or hilly areas. Behavior of components like energy sources, induction motors and power processing blocks deviate significantly from their normal behavior when driving in highly demanding situations. To tackle these shortcomings, non-linear controllers are preferred because of their efficiency. In literature, different controllers have been proposed for either the energy sources or the induction motor separately, whereas this research work focuses on a unified hybrid electric vehicle (HEV) model to simultaneously control the energy sources and the induction motor. The model used is a complete representation of electric system of FHEV and increases the performance of the vehicle. This unified model provides improved DC bus voltage regulation along with speed tracking when subjected to European extra urban drive cycle (EUDC). In this work, Robust Integral Backstepping and Robust Backstepping controllers have been designed. Lyapunov based analysis ensures the global stability of the system. Performance of proposed controllers is validated in MATLAB/Simulink environment. A comparative analysis is also given to illustrate the importance of the unified model proposed in this work.

INDEX TERMS Hybrid electric vehicles, unified model, non-linear control, integral backstepping control, backstepping control, stabilizing functions.

I. INTRODUCTION

Carbon dioxide (CO_2) makes 65% of the global greenhouse gases and its majority portion is attributed to transport industry [1]. The carbon footprint of renewable energy sources is far less as compared to conventional fossil fuels or natural gas resources. So, a lot of research is focused on the utilization of these renewable energy sources to mitigate the global environmental losses [2]. Rapid decline in fuel reserves and a rise in demand of personal vehicles have increased the necessity of eco-friendly and greener transport system.

Plugin hybrid electric vehicles (PHEV), battery electric vehicles (BEV) and fuel cell hybrid electric vehicles (FHEV) serve as a solution to the problems of fuel crisis and pollution related environmental issues [3], [4]. BEVs and PHEVs both need electricity from grid to charge the batteries. The major downside of these two types is that the setup costs of charging stations is too high and overall power generation is required to be increased in order to facilitate the rapid charging of the batteries [5]. On the other hand, FHEVs have no internal combustion engine (ICE) and have an electric motor, hence they are also emission free [6]. FHEVs have significant advantage over the other two types in terms of their long driving range and reliability [7].

ICE based vehicles have proven their stability and reliability in toughest terrains and offer a long driving range. In order to be widely accepted as a replacement of ICE based vehicles, electric vehicles need performance and driving range that is similar to or even better than that of conventional vehicles. FHEVs promise longer driving range and better performance in rough driving conditions when hybrid of fuel cell and energy storage devices is used. Fuel cells alone don't have the capability to meet the requirements of dynamic driving range, hence FHEVs use different combinations of fuel cells, ultracapacitor and battery. There are still a few challenges that are required to be addressed before these vehicles can be commercially realized on large scale [8].

The associate editor coordinating the review of this manuscript and approving it for publication was Lei Wang.

In order to improve the performance of HEVs, it is necessary that the current tracking of the energy sources and the speed tracking of the motor are robust and accurate. A number of linear controllers have been implemented on FHEVs in order to enhance their performance like Model Predictive Control, Fuzzy logic control and Proportional Integral (PI) control [9]–[12]. The performance of these linear controllers is acceptable but due to inherent limitations of the linear controllers, the operating range of the vehicle is significantly reduced.

Slippery roads, uphill/downhill drive, sudden acceleration or braking and frequent start-stops make driving experience very demanding and dynamic. The energy sources, power converters and the induction/traction motor of HEVs are dominated by non-linearities because of these high dynamic requirements. Hence the HEV models are usually complex and nonlinear in nature. Performance of nonlinear controllers for a dynamic nonlinear models is better than that of linear controllers because linear controllers fail to take into account the system non-linearities and are only stable when the system operates in a limited operating range [13], [14]. On the other hand, nonlinear controllers consider all the parameter deviations of the model. So, increased operating range of the model and global stability of the system is ensured [15]. Parallel Hybrid Energy Storage System (HESS) modeling and control has been done in [16]. With regards to nonlinear controllers, Lyapunov based controller has been proposed in [17] and sliding mode controller for FHEV has been proposed in [18].

FHEV modeled with fuel cell and ultracapacitor based HESS have been proposed in [19], [20], whereas ultracapacitor and battery based HESS in [21]. An updated model which uses all three sources: fuel cell, ultracapacitor and battery as HESS has been proposed in [17], [22]. This model uses fuel cell as primary source while ultracapacitor and battery act as auxiliary sources to store energy. This model offers increased energy storage capacity and high current and energy density [23].

In hybrid electric vehicles, meeting the dynamic load demands is the sole responsibility of energy sources which operate at different voltage levels and ensure the provision of desired DC bus voltage for a smooth ride. The electric motor is responsible for speed tracking under a dynamic load torque and has a wide operating range. Power converters play a vital role in efficient voltage regulation and serve as an interface between different energy sources and the induction motor. Different converter topologies have been proposed for these three sources in [24], [25]. Single bi-directional DC-DC converter, flyback converter and multi-device interleaved DC-DC converters have been proposed in [26]–[28]. In [26], [27] separate power converters for each source has been proposed. This is known as multiple converter topology and is more costly. Multi-input multi-output (MIMO) converter topology has been proposed in [29] is a cost effective alternative but is more complex than multiple converter topology.

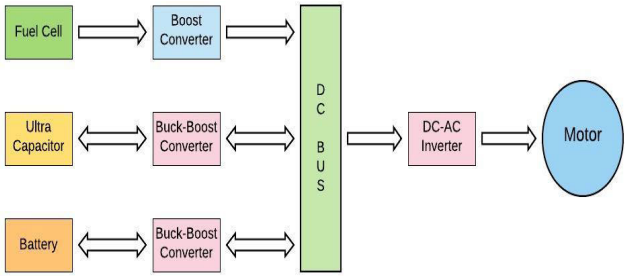

FIGURE 1. Block diagram of HEV.

The aim of this work is to improve the performance and driving experience of FHEV to the level of conventional ICE based vehicles. FHEV under study has a 3 phase induction motor and three energy sources; Fuel Cell, Ultracapacitor and a Battery. In literature the energy sources part has been the main focus for improvement of performance of vehicle and controller has been designed separately for energy sources and the induction motor part. Nonlinear control for FHEV energy sources part has been proposed in [17], [19], [20], [30] and it only improves DC bus voltage without taking into account the motor dynamics which is the main factor for load demand on the bus voltage. Here a complete unified model is proposed which improves the overall performance of the vehicle, while keeping in view the current limitations of the energy sources and the load torque of the motor. This model not only performs better regulation of the DC bus voltage, but also tracks the desired European Extra Urban Drive Cycle (EUDC) speed efficiently with perfect tracking of energy sources' current.

In this paper (a) backstepping, (b) robust backstepping/backstepping integrated with Sliding Mode Controller (SMC), (c) integral backstepping and (d) robust integral backstepping/integral backstepping integrated with SMC have been proposed. A comparative analysis of the conventional FHEV model and the proposed unified model, along with a comparison of the aforementioned nonlinear controllers on the proposed model using Matlab/Simulink have also been given.

This article has been organized as; Section II gives brief description of the system under study; sections III and IV give mathematical modeling of unified FHEV model while nonlinear control laws are formulated in section V; section VI discusses performance of FHEV under proposed controllers and the conclusion is given in section VII.

II. SYSTEM UNDER STUDY

The three important parts of FHEV are hybrid energy storage system (HESS), power converters and traction motor.

A. HYBRID ENERGY STORAGE SYSTEM

Three energy sources of FHEV are fuel cell (FC), ultracapacitor and battery. FC alone can not provide a smooth driving experience as it is unable to meet the load requirements alone. It is always used as a primary source along with one or

two secondary sources. Significance of all the energy sources used in this model is discussed in this section briefly.

1) FUEL CELL

Fuel cells have higher conversion efficiency and their fuel flexibility is more than internal combustion engines (ICE) vehicles but they have cold start-up and poor transient response [31]. There are many types of fuel cells used in literature like Solid oxide FC, alkaline FC, molten carbonate FC, phosphoric acid FC and proton exchange membrane fuel cells (PEMFC) [32]. PEMFC has found its application in vehicular technology because it has longer life, smaller size, higher efficiency and its working temperature is lower with better durability and shock resistance than other fuel cells [33], [34].

In order to overcome the deficiencies of fuel cells, auxiliary sources are used with them which improves the driving range and reduces the load stress on individual sources is also reduced. As a result, the life of the sources is also extended. To meet the transients and start up requirements, different combinations of FC, photovoltaic, ultracapacitor and battery are proposed in [35]–[38].

2) ULTRACAPACITOR

Ultracapacitor's high power density, small size, less charge time and its ability to capture maximum regenerative energy makes it a perfect candidate for use in FHEV [39]. The life of ultracapacitors is also more than battery having a range of about 1 million recharge cycles. In battery based electric vehicles, peak current during acceleration and high load torque is provided by ultracapacitors which relieves the stress on battery and hence battery life is extended [40].

3) BATTERY

Fuel cells have a slow start-up and ultracapacitors have problem of self-discharging, making battery a vital component in FHEV for initial traction. Although batteries have high energy storage density but their operation or recharge cycles are quite limited in comparison to ultracapacitors. Normally battery recharge cycles range from 800 to 2000 cycles depending upon the type of battery [41].

As each of these three energy sources complement each other, this combination of energy sources in FHEV proves to be a viable solution to the general shortcomings of electric vehicles.

B. ELECTRIC MOTORS

Tough driving conditions require a motor that can operate efficiently under dynamic load requirements. Choice of a suitable motor for electric vehicle plays a vital role in vehicle's performance. Electric motors have fast acceleration and their torque is more accurate than internal combustion engines [42]. Several types of electric motors are available in market like DC motors, induction motors, brush-less permanent magnet motors and switched reluctance motors, but the induction motors have proven to be better suited for their use in vehicular technology. Due to cost effectiveness, easy availability and wide speed range, they are preferred over other types of motors in electric and hybrid electric vehicles [43], [44].

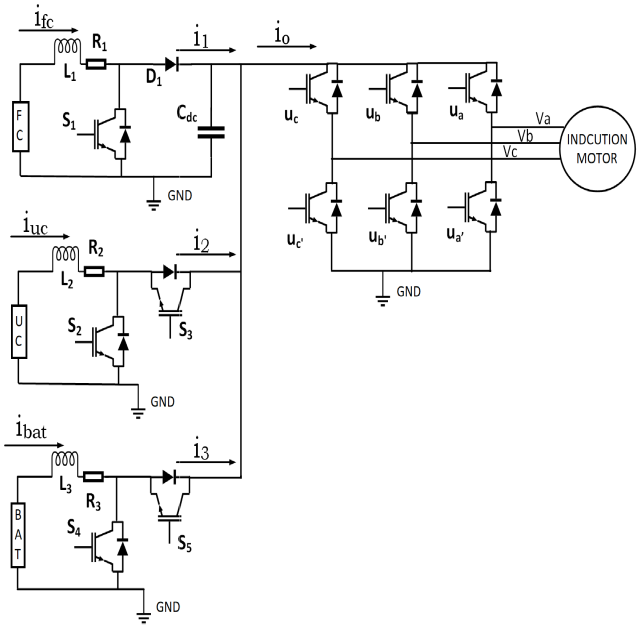

FIGURE 2. Electric circuit of power processing block.

III. MATHEMATICAL MODEL OF ELECTRIC POWER STAGE

The circuit diagram of unified model of FHEV is shown in figure 2. A DC-DC boost converter is used for fuel cell whereas; a bi-directional DC-DC buck-boost converter is used for both the ultracapacitor and the battery. A 3-phase DC-AC converter is used for electric motor. The model of FHEV has been derived using basic electric circuit laws on energy sources and power converters.

The output voltage of DC-DC bus (v_{dc}) appears across the output capacitor C_{dc}. $u_a, u_b, u_c, u_{a'}, u_{b'}, u_{c'}$ are the 3-phase inverter switching control inputs. They are used to obtain 3-phase DC-AC signal for driving the induction motor.

A. FUEL CELL - BOOST CONVERTER MODEL

Fuel cells lack the capability to utilize the regenerative braking or the excess power from any other sources, so unidirectional DC-DC boost converter is sufficient for this source. This converter consists of an insulated gate bipolar transistor (IGBT) switch S_1 shown in fig (2) and its value can be 0 or 1. There are two operation modes of this converter which depend upon the position of switch S_1. Following equations can be obtained after applying Kirchhoff's laws to boost converter:

$$\frac{di_{fc}}{dt} = -(1-u_1)\frac{v_{dc}}{L_1} - \frac{R_1}{L_1}i_{fc} + \frac{v_{fc}}{L_1} \tag{1}$$

$$\frac{dv_{dc}}{dt} = (1-u_1)\frac{i_{fc}}{C_{dc}} - \frac{i_1}{C_{dc}} \tag{2}$$

also

$$i_o = i_1 + i_2 + i_3 \tag{3}$$

where

$$i_2 = u_{23} i_{uc} \tag{4}$$

and

$$i_3 = u_{45} i_{bat} \tag{5}$$

where i_1, i_2 and i_3 represent the output currents of fuel cell, ultracapacitor and that of battery converters respectively. i_{fc}, i_{uc} and i_{bat} are fuel cell, ultracapacitor and battery input currents respectively and v_{dc} is output bus voltage. u_1 is the duty cycle of switch S_1.
Equation (2) can be written as

$$\frac{dv_{dc}}{dt} = (1-u_1)\frac{i_{fc}}{C_{dc}} - \frac{i_o}{C_{dc}} + \frac{i_{uc}}{C_{dc}}u_{23} + \frac{i_{bat}}{C_{dc}}u_{45} \tag{6}$$

B. ULTRACAPACITOR - BUCK-BOOST CONVERTER MODEL

Ultracapacitor can store the access charge of fuel cell and the energy from regenerative braking. To use ultracapacitor as an energy source and to charge it when required, a bidirectional DC-DC buck-boost converter is used as shown in figure 2. This buck-boost converter has two IGBT switches S_2 and S_3. The converter acts as a boost converter in order to meet the peak power demands and as a buck converter to store energy from regenerative braking. Boost mode refers to the discharging of the ultracapacitor and buck mode represents the charging. Equations (7) and (8) represent the boost and buck modes of the converter respectively. In boost mode, the switch S_2 is on while input to S_3 is zero, whereas in buck mode the condition reverses. In this mode Kirchhoff's laws give

$$\frac{di_{uc}}{dt} = \frac{v_{uc}}{L_2} - \frac{R_2}{L_2}i_{uc} - (1-u_2)\frac{v_{dc}}{L_2} \tag{7}$$

$$\frac{di_{uc}}{dt} = \frac{v_{uc}}{L_2} - \frac{R_2}{L_2}i_{uc} - u_3\frac{v_{dc}}{L_2} \tag{8}$$

Both of these equations can be written in a more compact form with the introduction of a variable j and the average control input u_{23} is defined as:

$$u_{23} = [j(1-u_2) + (1-j)u_3] \tag{9}$$

So, equations (7) and (8) take the form

$$\frac{di_{uc}}{dt} = \frac{v_{uc}}{L_2} - \frac{R_2}{L_2}i_{uc} - u_{23}\frac{v_{dc}}{L_2} \tag{10}$$

C. BATTERY - BUCK-BOOST CONVERTER MODEL

The battery operation is almost same as that of the ultracapacitor, the equations are obtained in a similar way. Boost and buck modes of the battery power converter are given by equation (11) and (12) respectively as:

$$\frac{di_{bat}}{dt} = \frac{v_{bat}}{L_3} - \frac{R_3}{L_3}i_{bat} - (1-u_4)\frac{v_{dc}}{L_3} \tag{11}$$

$$\frac{di_{bat}}{dt} = \frac{v_{bat}}{L_3} - \frac{R_3}{L_3}i_{bat} - u_5\frac{v_{dc}}{L_3} \tag{12}$$

Similarly, to write these equations in a compact form, a variable k is introduced. The average control input u_{45} is defined as:

$$u_{45} = [k(1-u_4) + (1-k)u_5] \tag{13}$$

and equations (11) and (12) take the form

$$\frac{di_{bat}}{dt} = -u_{45}\frac{v_{dc}}{L_3} - \frac{R_3}{L_3}i_{bat} + \frac{v_{bat}}{L_3} \tag{14}$$

D. COMBINED INVERTER-MOTOR MODEL

For tracking the speed of vehicle under changing load torque, Field Oriented Control (FOC) strategy is used. In this strategy, input power parameters are processed using a 3-phase DC-AC inverter due to which the induction motor is controlled indirectly.

The d-q axis rotated frame transformed mathematical model of the induction motor is given in [45] by equations (15)-(19).

$$\frac{di_{sd}}{dt} = ba\phi_{rd} + bp\Omega\phi_{rq} - \Upsilon i_{sd} + \omega i_{sq} + m_1 v_{sd} \tag{15}$$

$$\frac{di_{sq}}{dt} = ba\phi_{rq} - bp\Omega\phi_{rd} - \Upsilon i_{sq} - \omega i_{sd} + m_1 v_{sq} \tag{16}$$

$$\frac{d\phi_{rd}}{dt} = -a\phi_{rd} + (\omega_s - p\Omega)\phi_{rq} + aM_{sr}i_{sd} \tag{17}$$

$$\frac{d\phi_{rq}}{dt} = -a\phi_{rq} - (\omega_s - p\Omega)\phi_{rd} + aM_{sr}i_{sq} \tag{18}$$

$$\frac{d\Omega}{dt} = m(\phi_{rd}i_{sq} - \phi_{rq}i_{sd}) - c\Omega - \frac{T_l}{J} \tag{19}$$

where i_{sd} and i_{sq} are current components of stator's d-axis and q-axis respectively. Rotor flux d-axis and q-axis components are represented by ϕ_{rd} and ϕ_{rq}. Load torque, stator frequency and angular speed are represented by T_l, ω_s and Ω respectively. The number of pole-pairs is denoted by p and where

$$a = \frac{R_r}{L_r}, \quad b = \frac{M_{sr}}{L_s L_r \sigma}, \quad \sigma = 1 - \frac{M_{sr}^2}{L_s L_r}$$

$$\Upsilon = \frac{L_r^2 R_s + M_{sr}^2 R_r}{\sigma L_s L_r^2}, \quad m_1 = \frac{1}{L_s \sigma}$$

$$m = \frac{pM_{sr}}{JL_r}, \quad c = \frac{f_v}{J}$$

where L_r, L_s, R_r and R_s are rotor and stator self-inductances and resistances respectively. Mutual inductance between stator and rotor windings is M_{sr}. J gives inertia of the motor and load; coefficient of viscous damping is represented by f_v.

The two switching inputs of 3-phase inverter are given as u_d and u_q in d-q axis rotating frame transformed mathematical model. The currents and voltages of d-axis and q-axis of the inverter are as follows:

$$v_{dc} i_o = i_{sd} v_{sd} + i_{sq} v_{sq} \tag{20}$$

and the relations between inputs and outputs in term of switching inputs are

$$v_{sd} = u_d v_{dc} \tag{21}$$

and

$$v_{sq} = u_q v_{dc} \tag{22}$$

Equation (6) can be simplified using equations (20), (21) and (22) taking the form

$$\frac{dv_{dc}}{dt} = (1-u_1)\frac{i_{fc}}{C_{dc}} + u_{23}\frac{i_{uc}}{C_{dc}} + u_{45}\frac{i_{bat}}{C_{dc}} - u_d\frac{i_{sd}}{C_{dc}} - u_q\frac{i_{sq}}{C_{dc}} \tag{23}$$

where u_d and u_q are the input signals of the inverter for the d-q axis for motor control.

IV. UNIFIED MODEL OF FHEV

The complete mathematical model of FHEV is given in equations (24) through (32). These equations represent the unified model of FHEV with mathematical modeling of the energy sources and the motor. All these controlled variables are interlinked directly or indirectly. Renaming the following variables as

$$x_1 = i_{fc}, \quad x_2 = i_{uc}, \; x_3 = i_{bat}, \; x_4 = v_{dc}$$
$$x_5 = i_{sd}, \quad x_6 = i_{sq}, \; x_7 = \phi_{rd}, \; x_8 = \phi_{rq}, \; x_9 = \Omega$$

So, we get

$$\dot{x}_1 = -(1-u_1)\frac{x_4}{L_1} - \frac{R_1}{L_1}x_1 + \frac{v_{fc}}{L_1} \tag{24}$$

$$\dot{x}_2 = -u_{23}\frac{x_4}{L_2} - \frac{R_2}{L_2}x_2 + \frac{v_{uc}}{L_2} \tag{25}$$

$$\dot{x}_3 = -u_{45}\frac{x_4}{L_3} - \frac{R_3}{L_3}x_3 + \frac{v_{bat}}{L_3} \tag{26}$$

$$\dot{x}_4 = (1-u_1)\frac{x_1}{C_{dc}} + u_{23}\frac{x_2}{C_{dc}} + u_{45}\frac{x_3}{C_{dc}} - u_d\frac{x_5}{C_{dc}} - u_q\frac{x_6}{C_{dc}} \tag{27}$$

$$\dot{x}_5 = bax_7 + bpx_9x_8 - \Upsilon x_5 + \omega_s x_6 + m_1 u_d x_4 \tag{28}$$

$$\dot{x}_6 = bax_8 - bpx_9x_7 - \Upsilon x_6 - \omega_s x_5 + m_1 u_q x_4 \tag{29}$$

$$\dot{x}_7 = -ax_7 + (\omega_s - px_9)x_8 + aM_{sr}x_5 \tag{30}$$

$$\dot{x}_8 = -ax_8 - (\omega_s - px_6)x_7 + aM_{sr}x_6 \tag{31}$$

$$\dot{x}_9 = m(x_7x_6 - x_8x_5) - cx_9 - \frac{T_l}{J} \tag{32}$$

x_1 through x_3 are the averaged current values of fuel cell, ultracapacitor and battery respectively, while x_4 is the DC bus voltage. x_5 and x_6 represent d-axis and q-axis stator currents respectively, whereas d-axis and q-axis rotor flux are represented by x_7 and x_8 respectively. The angular speed of the induction motor is represented by x_9. The difference between the conventional FHEV model and the unified model can easily be observed. The dynamics of the energy sources depend on DC bus, whereas the dynamics of the DC bus here also incorporates the motor input current dynamics. The motor current dynamics are linked with the dynamics of motor flux and angular speed of motor as well.

V. CONTROLLER DESIGN

The proposed nonlinear controller for FHEV should be able to fulfill the following objectives efficiently in order to be considered effective:

- Voltage regulation of DC bus with varying load,
- Currents tracking of energy sources to their reference values,
- Speed tracking of induction motor to its reference value,
- Global assymptotic stability of the controlled system.

As the boost converter of FC has non-minimum phase nature, we can not directly track the reference value of DC bus voltage. The DC bus voltage and FC current are linked to each other such that if FC current tracks its reference value i_{fc}, DC bus tracks reference voltage v_{dc}. The relationship of these reference values is given in the following equations:

$$P_{in} = P_{out} \tag{33}$$

$$P_{fc} + P_{uc} + P_{bat} = P_{out} \tag{34}$$

The input and output powers of the system must be equal and the input power is the power of energy sources. P_{in} and P_{out} are the input and output powers respectively, whereas P_{fc}, P_{uc} and P_{bat} are fuel cell, ultracapacitor and battery powers respectively. Solving equation (34) for x_{1ref}, we have

$$x_{1ref} = \beta\left(\frac{v_{dcref}i_o - v_{uc}i_{uc} - v_{bat}i_{bat}}{v_{fc}}\right) \tag{35}$$

Here, x_{1ref} is the reference value of FC and β is the ideality factor which must have a value greater than 1. This factor is used to compensate the losses in power converters.

A. INTEGRAL BACKSTEPPING SLIDING MODE CONTROLLER DESIGN

In order to track the currents of energy sources to their reference values, corresponding error signals must be defined. The error in FC current is defined as:

$$e_1 = x_1 - x_{1ref} \tag{36}$$

Taking the time derivative of equation (36) to get its dynamics as

$$\dot{e}_1 = \dot{x}_1 - \dot{x}_{1ref} \tag{37}$$

Actual dynamics of the error can be found using equation (24) as

$$\dot{e}_1 = -(1-u_1)\frac{x_4}{L_1} - \frac{R_1}{L_1}x_1 + \frac{v_{fc}}{L_1} - \dot{x}_{1ref} \tag{38}$$

Adding integral action to the error e_1:

$$\zeta_1 = e_1 + \sigma \tag{39}$$

where

$$\sigma = \int_0^t (x_1 - x_{1ref})dt \tag{40}$$

e_1 given by equation (36) must approach zero for which the Lyapunov candidate function is chosen as,

$$V_1 = \frac{1}{2}e_1^2 + \frac{\kappa}{2}\sigma^2 \tag{41}$$

here κ is a positive constant. Time derivative of V_1 from equation (41) gives:

$$\dot{V}_1 = e_1\dot{e}_1 + \kappa\sigma\dot{\sigma} \tag{42}$$

Equation (40) gives:

$$\dot{\sigma} = e_1 \tag{43}$$

Using the value of $\dot{e_1}$ and $\dot{\sigma}$ from equations (38) and (43) respectively, equation (42) becomes:

$$\dot{V}_1 = e_1\left(\frac{-R_1}{L_1}x_1 + \frac{1}{L_1}v_{fc} - \frac{1-u_1}{L_1}x_4 - \dot{x}_{1ref} + \kappa\sigma\right) \tag{44}$$

To ensure that $\dot{V}_1$ stays negative definite, let us take

$$\frac{-R_1}{L_1}x_1 + \frac{1}{L_1}v_{fc} - \frac{1-u_1}{L_1}x_4 - \dot{x}_{1ref} + \kappa\sigma = -k_1e_1 \tag{45}$$

where the design parameter k_1 can have any positive constant value. Taking $\frac{x_4}{L_1}$ as virtual control and representing it by γ, we get

$$\gamma = \frac{\left(k_1e_1 + \frac{-R_1}{L_1}x_1 + \frac{1}{L_1}v_{fc} - \dot{x}_{1ref} + \kappa\sigma\right)}{1-u_1} \tag{46}$$

For the system to be stable, $\frac{x_4}{L_1} = \gamma$ must hold true at all times. Hence, defining e_2 as:

$$e_2 = \frac{x_4}{L_1} - \gamma \tag{47}$$

which must go to zero to ensure $\frac{x_4}{L_1} = \gamma$.

Using equation (47) and putting the value of virtual control $\frac{x_4}{L_1}$ in equation (38), we get

$$\dot{e_1} = \frac{-R_1}{L_1}x_1 + \frac{1}{L_1}v_{fc} - (1-u_1)(e_2+\gamma) - \dot{x}_{1ref} \tag{48}$$

Putting the value of γ from equation (46) in equation (48), we get:

$$\dot{e_1} = -\kappa\sigma - k_1e_1 - (1-u_1)e_2 \tag{49}$$

Now, equation (44) can be written as:

$$\dot{V}_1 = -k_1e_1^2 - (1-u_1)e_1e_2 \tag{50}$$

Time derivative of e_2 in equation (47) gives

$$\dot{e_2} = \frac{\dot{x}_4}{L_1} - \dot{\gamma} \tag{51}$$

Taking time derivative of γ from equation (46), we get:

$$\dot{\gamma} = \left(\frac{k_1\dot{e}_1 - \frac{R_1}{L_1}\dot{x}_1 + \frac{1}{L_1}\dot{v}_{fc} - \ddot{x}_{1ref} + \kappa e_1}{(1-u_1)}\right) + \frac{\dot{u}_1\gamma}{(1-u_1)} \tag{52}$$

To simplify the above expression, declaring a new variable for numerator of first term,

$$\zeta = k_1\dot{e}_1 - \frac{R_1}{L_1}\dot{x}_1 + \frac{1}{L_1}\dot{v}_{fc} - \ddot{x}_{1ref} + \kappa e_1 \tag{53}$$

Using equation (49) for value of $\dot{e}_1$, ζ can be expressed in terms of e_1 and e_2. Now, equation (52) can be written as:

$$\dot{\gamma} = \frac{\zeta}{(1-u_1)} + \frac{\dot{u}_1\gamma}{(1-u_1)} \tag{54}$$

Substituting the values of $\dot{x_4}$ and $\dot{\gamma}$ from equations (27) and (54) respectively in equation (51), we get:

$$\dot{e_2} = \frac{1}{L_1}\left[(1-u_1)\frac{x_1}{C_{dc}} + u_{23}\frac{x_2}{C_{dc}} + u_{45}\frac{x_3}{C_{dc}} - u_d\frac{x_5}{C_{dc}} - u_q\frac{x_6}{C_{dc}}\right] - \frac{\zeta}{(1-u_1)} - \frac{\dot{u}_1\gamma}{(1-u_1)} \tag{55}$$

Combined Lyapunov function is defined as follows for ensuring convergence of both the errors e_1 and e_2 to zero,

$$V_{c_1} = V_1 + \frac{1}{2}e_2^2 \tag{56}$$

Taking time derivative of equation (56), we have

$$\dot{V}_{c_1} = \dot{V}_1 + e_2\dot{e}_2 \tag{57}$$

Putting the value of $\dot{V}_1$ from equation (50), we get:

$$\dot{V}_{c_1} = -k_1e_1^2 - e_2[(1-u_1)e_1 - \dot{e}_2] \tag{58}$$

For making $\dot{V}_{c_1}$ negative definite, taking

$$(1-u_1)e_1 - \dot{e}_2 = k_2e_2 \tag{59}$$

where k_2 is design parameter of control and $k_2 > 0$ for all times. So, equation (58) becomes

$$\dot{V}_{c_1} = -k_1e_1^2 - k_2e_2^2 \tag{60}$$

Using $\dot{e}_2$ from equation (55) in equation (59) and solving for control law u_1, we get

$$\dot{u}_1 = \frac{(1-u_1)}{\gamma}\left[k_2e_2 + \frac{1}{L_1}\left((1-u_1)\frac{x_1}{C_{dc}} + u_{23}\frac{x_2}{C_{dc}} + u_{45}\frac{x_3}{C_{dc}} - u_d\frac{x_5}{C_{dc}} - u_q\frac{x_6}{C_{dc}}\right) - (1-u_1)e_1 - \frac{\zeta}{(1-u_1)}\right] \tag{61}$$

This control law would ensure tracking of x_1 and x_4 to their reference values x_{1ref} and x_{4ref} respectively.

To incorporate robustness in integral backstepping, a sliding surface is defined as:

$$S = a_1e_1 + a_2e_2 \tag{62}$$

Based on the surface S, adding a switching term in control law u_1 to formulate integral backstepping plus SMC controller. Using $\dot{u}_1$ from equation (61), the final control law u_1 becomes:

$$u_1 = \int_0^t \dot{u}_1dt - ks(sat(S/B)) \tag{63}$$

where B $\in [0, 1]$, $ks > 0$ and sat represents saturation function.

$$sgn(S) = \begin{cases} -1, & if\ x < 0 \\ 0, & if\ x = 0 \\ 1, & if\ x > 0 \end{cases} \tag{64}$$

Being approximation of signum function (sgn), saturation function (sat) turns out to be:

$$sat(S/\varepsilon) = \begin{cases} S/\varepsilon, & if \ \ |\ S/\varepsilon\ | \leq 1 \\ sgn(S/\varepsilon), & otherwise \end{cases} \tag{65}$$

To define the control law for the remaining energy sources, we need to find u_{23} for tracking x_2 to its reference value x_{2ref}. For ultracapacitor, following error term is introduced:

$$e_3 = x_2 - x_{2ref} \tag{66}$$

Taking time derivative of e_3 from equation (66) and substituting the value of $\dot{x_2}$ from equation (25), we get:

$$\dot{e_3} = -u_{23}\frac{x_4}{L_2} - \frac{R_2}{L_2}x_2 + \frac{v_{uc}}{L_2} - \dot{x}_{2ref} \tag{67}$$

Lyapunov candidate function of error e_3 is selected as:

$$V_2 = \frac{1}{2}e_3^2 \tag{68}$$

Taking time derivative of V_2 gives:

$$\dot{V}_2 = e_3\dot{e_3} \tag{69}$$

To make $\dot{V}_2$ negative definite, we take

$$\dot{e}_3 = -k_3 e_3 \tag{70}$$

so that equation (67) gives

$$-u_{23}\frac{x_4}{L_2} - \frac{R_2}{L_2}x_2 + \frac{v_{uc}}{L_2} - \dot{x}_{2ref} = -k_3 e_3 \tag{71}$$

So, equation (69) becomes:

$$\dot{V}_2 = -k_3 e_3^2 \tag{72}$$

Solving equation (71) for u_{23}, we get following control law:

$$u_{23} = \frac{1}{x_4}\left[L_2 k_3 e_3 - R_2 x_2 + v_{uc} - L_2\dot{x}_{2ref}\right] \tag{73}$$

The combined Lyapunov function is taken as,

$$V_{c_2} = V_{c_1} + V_2 \tag{74}$$

Taking time derivative of V_{c_2} and using equations (71) and (74) we get

$$\dot{V}_{c_2} = -k_1 e_1^2 - k_2 e_2^2 - k_3 e_3^2 \tag{75}$$

Similarly, for battery we need to find the control law u_{45} so that x_3 tracks its reference value x_{3ref}. Defining the following error for this purpose,

$$e_4 = x_3 - x_{3ref} \tag{76}$$

Taking time derivative of e_4 from equation (76)

$$\dot{e}_4 = \dot{x}_3 - \dot{x}_{3ref} \tag{77}$$

substituting the value of $\dot{x_3}$ from equation (26), we get:

$$\dot{e_4} = -u_{45}\frac{x_4}{L_3} - \frac{R_3}{L_3}x_3 + \frac{v_{bat}}{L_3} - \dot{x}_{3ref} \tag{78}$$

Lyapunov candidate function is defined as:

$$V_3 = \frac{1}{2}e_4^2 \tag{79}$$

Time derivative of V_3 gives:

$$\dot{V}_3 = e_4\dot{e_4} \tag{80}$$

For making $\dot{V}_3$ negative definite, we take

$$\dot{e}_4 = -k_4 e_4 \tag{81}$$

where $k_4 > 0$. So, equation (78) gives

$$-u_{45}\frac{x_4}{L_3} - \frac{R_3}{L_3}x_3 + \frac{v_{bat}}{L_3} - \dot{x}_{3ref} = -k_4 e_4 \tag{82}$$

Solving equation (82) for u_{45} in order to get the control law as

$$u_{45} = \frac{1}{x_4}\left[L_3 k_4 e_4 - R_3 x_3 + v_{bat} - L_3\dot{x}_{3ref}\right] \tag{83}$$

Combined Lyapunov function is taken as

$$V_{c_3} = V_{c_2} + V_3 \tag{84}$$

Its time derivative gives

$$\dot{V}_{c_3} = -k_1 e_1^2 - k_2 e_2^2 - k_3 e_3^2 - k_4 e_4^2 \tag{85}$$

For tracking motor speed and d-axis rotor flux, we need to design the control law u_d and u_q. Defining d-axis rotor flux error as follows

$$e_5 = x_7 - \phi_{rd}^* \tag{86}$$

and speed error is defined as,

$$e_6 = x_9 - \Omega_d \tag{87}$$

where ϕ_{rd}^* and Ω_d are represent corresponding reference values.

In order to implement field oriented control (FOC), it is necessary that the modulus of rotor flux is equal to the magnitude of d-axis component rotor flux. Following expression must be satisfied:

$$\sqrt{\phi_{rd}^2 + \phi_{rq}^2} = \|\ \phi_{rd}\ \| \tag{88}$$

It is only possible when q-axis component of rotor flux is made zero. Stator frequency ω_s is selected in such a way that it makes equation (31) exponentially zero, taking x_8 and its dynamics equal to zero. The effect of selection of this type of frequency is observed in design of control law.

$$\omega_s = px_6 + a\frac{M_{sr}}{x_7}x_6 \tag{89}$$

Taking time derivative of equation (86) gives

$$\dot{e}_5 = \dot{x}_7 - \dot{\phi^*}_{rd} \tag{90}$$

Putting the value of $\dot{x}_7$ from equation (30) in equation (90), we get:

$$\dot{e}_5 = -ax_7 + aM_{sr}x_5 - \dot{\phi^*}_{rd} \tag{91}$$

Lyapunov candidate function is taken as:

$$V_4 = \frac{1}{2}e_5^2 \tag{92}$$

Taking time derivative of equation (92), we get:

$$\dot{V}_4 = e_5\dot{e_5} \tag{93}$$

For making $\dot{V}_4$ negative definite we put

$$\dot{e_5} = -k_5e_5 \tag{94}$$

where $k_5 > 0$. So, equation (91) gives

$$-ax_7 + aM_{sr}x_5 - \dot{\phi^*}_{rd} = -k_5e_5 \tag{95}$$

Taking x_5 in equation (95) as virtual controller x_{5d} and solving for it,

$$x_{5d} = \frac{1}{aM_{sr}}(-k_5e_5 + ax_7 + \dot{\phi^*}_{rd}) \tag{96}$$

Stability is ensured only when $x_{5d} = x_5$, so defining another error,

$$e_7 = x_5 - x_{5d} \tag{97}$$

from here,

$$x_5 = e_7 + x_{5d} \tag{98}$$

Putting value of x_5 from equation (98) in equation (91), we get:

$$\dot{e_5} = -k_5e_5 + aM_{sr}e_7 \tag{99}$$

Substituting $\dot{e_5}$ from equation (99) in equation (93). $\dot{V}_4$ becomes,

$$\dot{V}_4 = -k_5e_5^2 + e_5(aM_{sr}e_7) \tag{100}$$

Dynamical error of e_7 is obtained by taking the time derivative of equation (97), we get:

$$\dot{e_7} = \dot{x_5} - \dot{x_{5d}} \tag{101}$$

Putting $\dot{x_5}$ from equation (28) in above equation, we have

$$\dot{e_7} = bax_7 - \Upsilon x_5 + \omega_s x_6 + m_1u_dx_4 - \dot{x_{5d}} \tag{102}$$

Let us define the Lyapunov candidate function as,

$$V_5 = V_4 + \frac{1}{2}e_7^2 \tag{103}$$

Taking time derivative of V_5 and substituting value of $\dot{V}_4$ from equation (100), we get:

$$\dot{V}_5 = -k_5e_5^2 + e_7(e_5aM_{sr} + \dot{e_7}) \tag{104}$$

For making equation (104) negative definite, let us take design parameter $k_7 > 0$ such that:

$$e_5aM_{sr} + \dot{e_7} = -k_7e_7 \tag{105}$$

so,

$$\dot{V}_5 = -k_5e_5^2 - k_7e_7^2 \tag{106}$$

Now, using the value of $\dot{e_7}$ from equation (102) and solving for u_d, we get

$$u_d = \frac{1}{m_1x_4}(-k_7e_7 - aM_{sr}e_5 - bax_7 + \Upsilon x_5 - \omega_s x_6 + \dot{x_{5d}}) \tag{107}$$

To find u_q, taking time derivative of equation (87), we have

$$\dot{e_6} = \dot{x_9} - \dot{\Omega}_d \tag{108}$$

Substituting $\dot{x_9}$ from equation (32) in equation (108), we get:

$$\dot{e_6} = mx_7x_6 - cx_9 - \frac{T_l}{J} - \dot{\Omega}_d \tag{109}$$

Taking Lyapunov candidate function as:

$$V_6 = \frac{1}{2}e_6^2 \tag{110}$$

Time derivative of equation (110) gives:

$$\dot{V}_6 = e_6\dot{e_6} \tag{111}$$

In order to make $\dot{V}_6$ negative definite, we put

$$\dot{e_6} = -k_6e_6 \tag{112}$$

where $k_6 > 0$. So, equation (109) gives

$$mx_7x_6 - cx_9 - \frac{T_l}{J} - \dot{\Omega}_d = -k_6e_6 \tag{113}$$

Replacing x_6 in equation (113) as virtual controller x_{6d} and solving for it, we get

$$x_{6d} = \frac{1}{mx_7}(-k_6e_6 + cx_9 + \frac{T_l}{J} + \dot{\Omega}_d) \tag{114}$$

To ensure stability, $x_{6d} = x_6$ must hold true. So, defining another error,

$$e_8 = x_6 - x_{6d} \tag{115}$$

Rearranging to get x_6, as

$$x_6 = e_8 + x_{6d} \tag{116}$$

Substituting the value of x_6 from equation (116) in equation (109), following expression is obtained:

$$\dot{e_6} = -k_6e_6 + mx_7e_8 \tag{117}$$

Putting $\dot{e_6}$ from above in equation (111). $\dot{V}_6$ becomes,

$$\dot{V}_6 = -k_6e_6^2 + e_6(mx_7e_8) \tag{118}$$

Taking time derivative of equation (123) gives:

$$\dot{e_8} = \dot{x_6} - \dot{x_{6d}} \tag{119}$$

Substituting $\dot{x_6}$ from equation (29) in equation (119), we have

$$\dot{e_8} = -bpx_9x_7 - \Upsilon x_6 - \omega_s x_5 + m_1u_qx_4 - \dot{x_{6d}} \tag{120}$$

Defining the Lyapunov candidate function as,

$$V_7 = V_6 + \frac{1}{2}e_8^2 \tag{121}$$

Substituting value of $\dot{V}_6$ from equation (118) after taking time derivative of equation (121) as,

$$\dot{V}_7 = -k_6 e_6^2 + e_8(e_6 m x_7 + \dot{e}_8) \tag{122}$$

In order to make $\dot{V}_7$ negative definite, we put

$$e_6 m x_7 + \dot{e}_8 = -k_8 e_8 \tag{123}$$

where $k_8 > 0$, so

$$\dot{V}_7 = -k_6 e_6^2 - k_8 e_8^2 \tag{124}$$

Now, substituting $\dot{e}_8$ from equation (120) in equation (123) and solving for u_q

$$u_q = \frac{1}{m_1 x_4}(-k_8 e_8 - m x_7 e_6 + bp x_9 x_7 + \Upsilon x_6 + \omega_s x_5 + \dot{x}_{6d}) \tag{125}$$

Combined Lyapunov function becomes,

$$V_c = V_{c_3} + V_5 + V_7 \tag{126}$$

Taking time derivative of V_c and using equations (106) and (124), we get:

$$\dot{V}_c = -k_1 e_1^2 - k_2 e_2^2 - k_3 e_3^2 - k_4 e_4^2 - k_5 e_5^2 - k_6 e_6^2 - k_7 e_7^2 - k_8 e_8^2 \tag{127}$$

$$\dot{V} = \sum_{i=1}^{8} -k_i e_i^2 \tag{128}$$

From above equation, global stability of the system is ensured.

B. BACKSTEPPING PLUS SMC CONTROLLER DESIGN

In integral backstepping, an integral term is added to error e_1. If integral action is not included in the error, equation (45) becomes:

$$\frac{-R_1}{L_1} x_1 + \frac{1}{L_1} v_{fc} - \frac{1 - u_1}{L_1} x_4 - \dot{x}_{1ref} = -k_1 e_1 \tag{129}$$

Following the same steps as done in sub section V-A, virtual control law γ for backstepping controller gets updated as follows:

$$\gamma = \frac{\left(k_1 e_1 + \frac{-R_1}{L_1} x_1 + \frac{1}{L_1} v_{fc} - \dot{x}_{1ref}\right)}{1 - u_1} \tag{130}$$

This γ will only affect our control law u_1. All other equations remain same as for integral backstepping.

In order to incorporate robustness, equations (62) and (63) can be used. Resulting control law u_1 will constitute Backstepping plus SMC controller.

VI. SIMULATION RESULTS

The unified model with proposed controllers is simulated in Matlab/Simulink environment. Tables 1, 2 and 3 represent specifications of energy sources, converter and electric motor respectively.

TABLE 1. Energy sources.

Component	Specifications
PEMFC	350 V, 250 A, 34 kW
UC module	205 V dc, 2700 F
Battery Module	288 V dc, 13.9 Ah, Li-ion

TABLE 2. Converter specifications.

Component	Specifications
Inductance L_1, L_2 and L_3	$3.3mH$
Inductance's ESRs R_1 , R_2 and R_3	$20m\Omega$
Output Capacitor C_{out}	$1.66mF$
Switching Frequency	$20khz$
Ideality Factor (β)	1.014

TABLE 3. Electric motor.

Component	Specification
Motor Type	3-phase induction motor
Nominal Power	$7.5kW$
Nominal Voltage	$380V$
Nominal frequency	$50hz$
Nominal flux	$1Wb$
Nominal Power	$7.5kW$
R_r	0.93Ω
R_s	1.633Ω
L_r	$0.076H$
L_s	$0.142H$
f_v	$0.0018\frac{Nm.s}{rad}$
M_{sr}	$0.099H$
p	2
J	$0.0111\frac{Nm.s^2}{rad}$

A. PROPORTIONAL INTEGRAL (PI) CONTROLLER

The supremacy of the proposed unified model over the conventional FHEV model is highlighted by the results of one of the most widely used linear control techniques. The models are subjected to same load profile as shown in figure 3.PI controller is applied to both the models and the results in figure 4 clearly show that the unified model performs better voltage regulation with similar control efforts for both the models.

Under the 10 second test, the unified model outperforms the conventional model significantly. As it is evident from figure 4, unified model is a better choice when it comes to efficient control of hybrid electric vehicles.

The conventional model of FHEV is given by equations (131 - 134). As conventional model does not include the motor dynamics, it fails to capture the true electrical nature of the system. Hence, the voltage regulation is not as efficient as unified model.

$$\dot{x}_1 = -(1 - u_1)\frac{x_4}{L_1} - \frac{R_1}{L_1} x_1 + \frac{v_{fc}}{L_1} \tag{131}$$

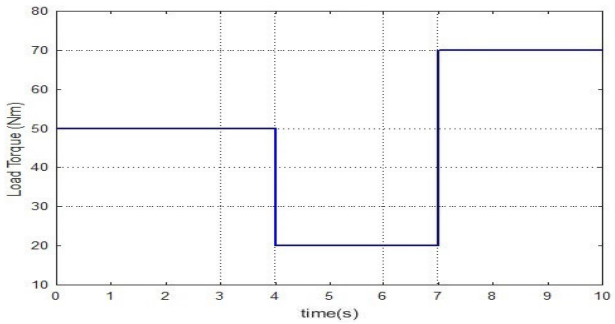

FIGURE 3. Load torque profile.

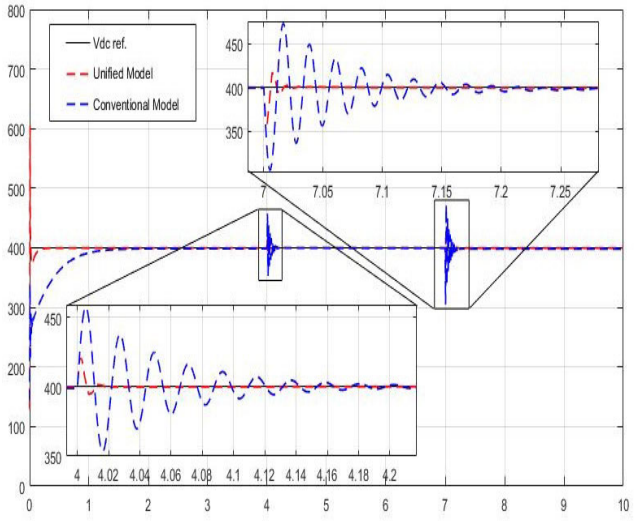

FIGURE 4. DC-DC bus voltage.

$$\dot{x}_2 = -u_{23}\frac{x_4}{L_2} - \frac{R_2}{L_2}x_2 + \frac{v_{uc}}{L_2} \tag{132}$$

$$\dot{x}_3 = -u_{45}\frac{x_4}{L_3} - \frac{R_3}{L_3}x_3 + \frac{v_{bat}}{L_3} \tag{133}$$

$$\dot{x}_4 = (1-u_1)\frac{x_1}{C_{dc}} + u_{23}\frac{x_2}{C_{dc}} + u_{45}\frac{x_3}{C_{dc}} - \frac{1}{C_{dc}}i_o \tag{134}$$

B. INTEGRAL BACKSTEPPING PLUS SMC

The controller has been subjected to EUDC. It represents the standard driving conditions in a city and is known for its high speed driving mode. In this profile a vehicle can take a maximum speed of 90 km/h and the speed of the profile refers to the load on the motor. Equations used to compute the power demand and corresponding load currents from DC bus voltage and ultimately the energy sources are as follows:

$$P_{out} = \frac{1}{0.75}\left[0.5p_a v_t^2 AC_x + MgC_r + M\frac{dv_t}{dt}\right]v_t \tag{135}$$

$$i_o = \frac{1}{(0.75)(400)}\left[0.5p_a v_t^2 AC_x + MgC_r + M\frac{dv_t}{dt}\right]v_t \tag{136}$$

where the working efficiency of the inverter is considered to be 75 percent. The vehicle speed is represented by v_t, standard air density by p_a, gravitational acceleration constant by g, mass of car by M and A is the front area of the car. The table 4 gives the parameters used in the equations (135) and (136).

TABLE 4. Specifications of vehicle parameters.

Parameter	Specifications
Car Mass M	1066Kg
Front Area (A)	$1.8m^2$
Switching frequency	100kHz
Passenger Weight (Two passengers)	70+70kg
Rolling resistance coefficient(C_r)	0.0048
Aerodynamic drag coefficient (C_x)	0.19

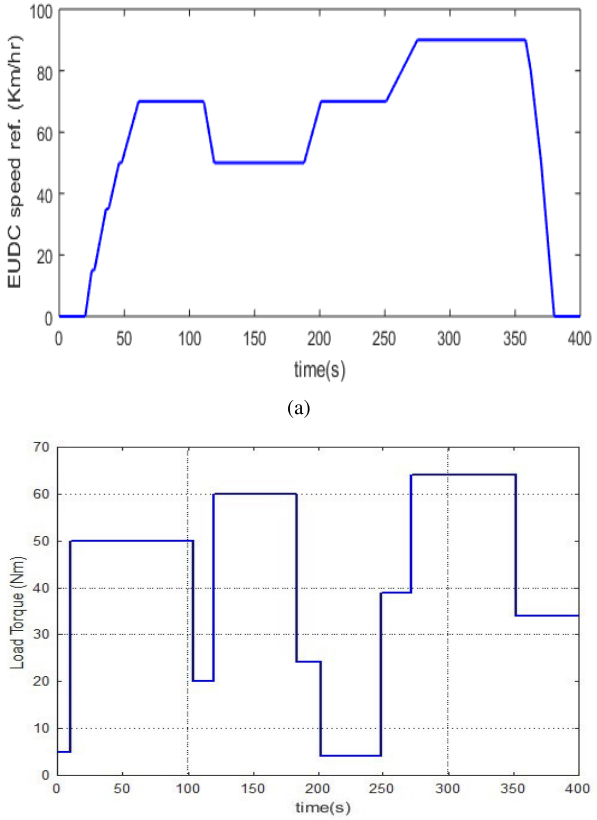

FIGURE 5. EUDC Cycle (a) speed reference (b) torque reference.

The EUDC speed profile is shown in figure 5(a), whereas figure 5(b) shows the load torque of motor or the torque reference. While driving, three modes of motor torque are of utmost importance: acceleration, deceleration/braking and steady speed. The load torque profile encompasses all three modes and the controller's functionality can be tested effectively.

The controller gains are selected on a trial and error basis, in which gains are chosen randomly and then checked for error values. Those having lesser error are selected as final gains given in table 5.

The switching control signals (duty ratio) of the control laws of energy sources are shown in figure 6, the load current

TABLE 5. Controller gains.

coefficient	value
B	0.5
κ	$1e^4$
a_1	$1e^{-3}$
a_2	$1e^{-3}$
k_s	$1e^{-3}$
k_1	$1e^3$
k_2	$1e^3$
k_3	$1e^3$
k_4	$1e^3$
k_5	$2e^3$
k_6	$3e^3$
k_7	$9e^3$
k_8	$6e^3$

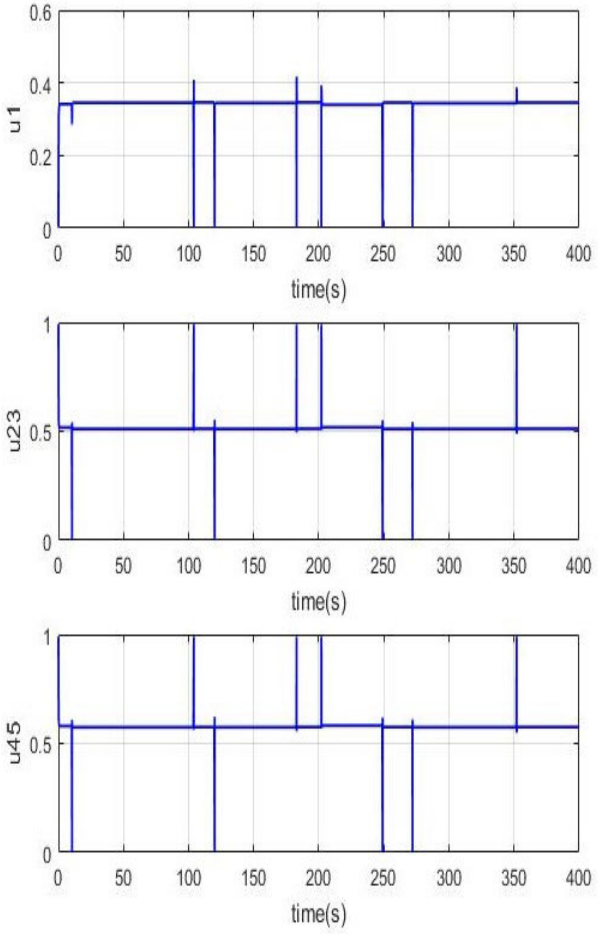

FIGURE 6. Converter control laws (a) u_1 (b) u_{23} (c) u_{45}.

profile is shown in figure 7. The currents of energy sources are shown in figure 8 and the corresponding current tracking errors of the energy sources are shown in figure 9. It can be clearly observed that the current tracking errors are not too large and are in an acceptable range because they do not

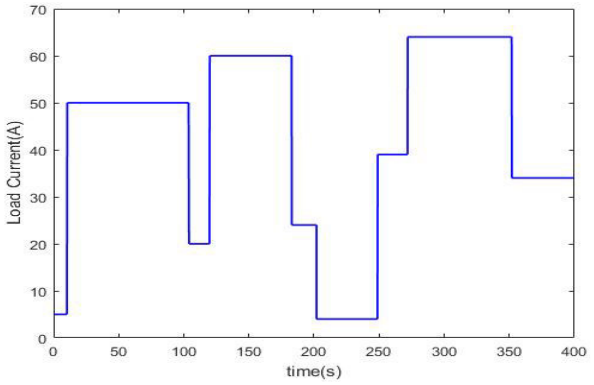

FIGURE 7. Load current profile.

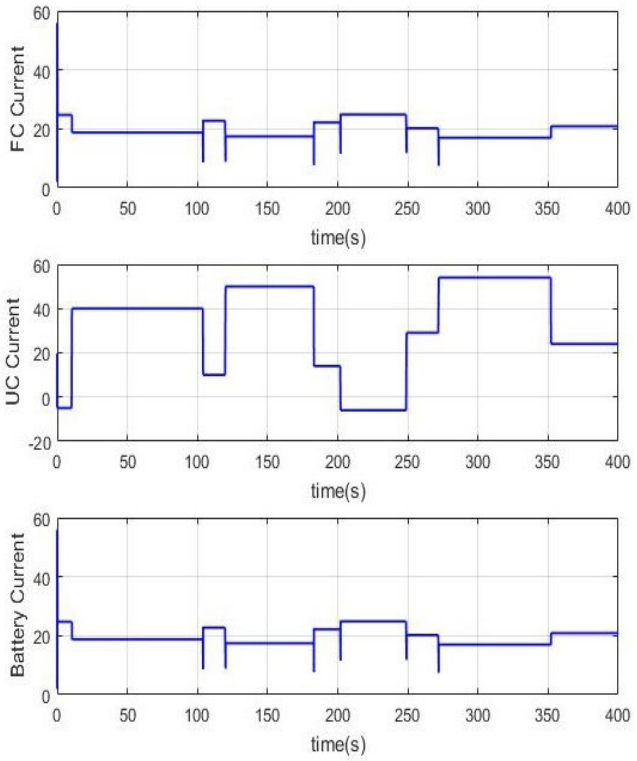

FIGURE 8. Energy sources' currents (a) Fuel Cell (b) Ultracapacitor (c) Battery.

violate any limitation of the energy sources. Besides, this work does not focus on energy management of the sources due to which the peaks are observed in the errors. The errors in figure 6(a), 6(b) and 6(c) refer to fuel cell error (e_1), ultracapacitor error (e_3) and battery error (e_4) respectively.

The control laws for the d-q axis motor are shown in figure 10. The control laws u_d and u_q are responsible for ensuring accurate speed tracking of the vehicle to the reference values by generating switching signals for the 3-phase inverter. These control laws generate appropriate voltages v_{sd} and v_{sq} across stator input, which in turn generates the motor input currents i_{sd} and i_{sq}.

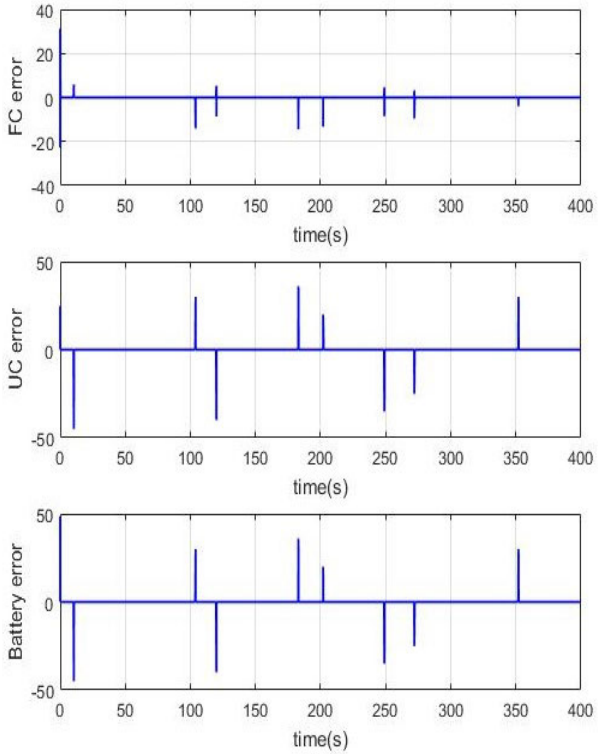

FIGURE 9. Current tracking error (a) Fuel Cell (b) Ultracapacitor (c) Battery.

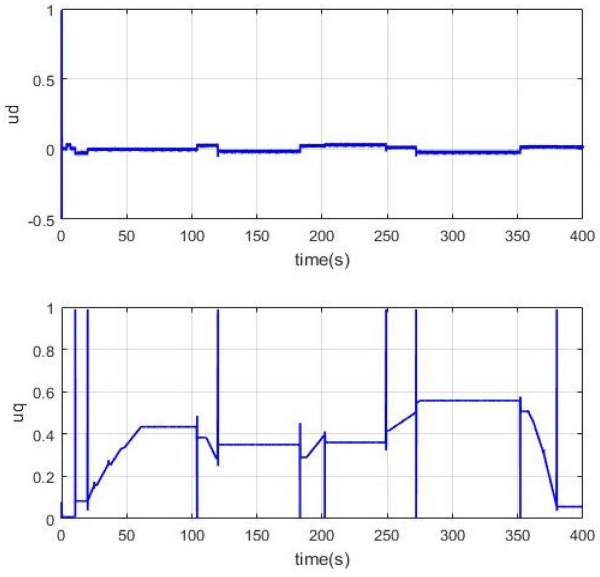

FIGURE 10. Motor control laws (a) u_d (b) u_q.

C. COMPARATIVE ANALYSIS

The main objectives of control design of FHEV include voltage regulation and accurate speed reference tracking. The controller which achieves these objectives more efficiently with lesser errors is considered to be better than the other controllers in comparison. In this work four nonlinear control controllers have been designed for the unified FHEV model: Integral Backstepping plus SMC (IBS+SMC), Integral Backstepping (IBS), Backstepping plus SMC (BS+SMC) and Backstepping (BS). The voltage of DC-DC bus is supposed to be 400 volts (V) under the dynamic load demands. The comparison of DC-DC bus voltage (V_{dc}) or x_4 for the aforementioned nonlinear controllers is shown in figure 11. The spikes in the graph correspond to the transitions or changes of motor speed in EUDC speed profile (fig 5). At all the transitions, the overshoots/undershoots of IBS+SMC are smaller and they are short-lived spikes with fast settling time. The steady state error of this controller is also lower than the other applied nonlinear controllers and convergence is very close to the targeted value of 400V.

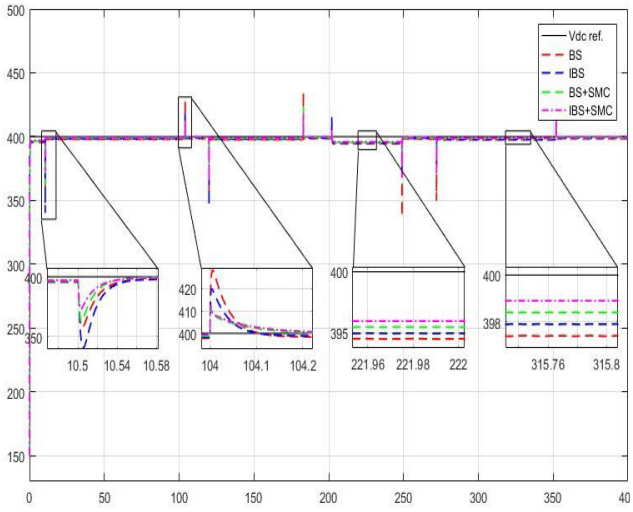

FIGURE 11. DC-DC bus voltage tracking (V_{dc}).

TABLE 6. Root mean square errors (RMSE).

Technique	RMSE V_{dc}	RMSE Speed Tracking
IBS+SMC	2.1078	0.0147
IBS	3.2117	0.0260
BS+SMC	3.3696	0.0269
BS	3.7789	0.0280
PID	8.4187	0.1890

The speed tracking of all the controller is very efficient but IBS+SMC produces the better results. At each transition, the overshoot/undershoot and the settling time of IBS+SMC is the less. A comparison of speed tracking of all the proposed controllers is shown in figure 12. The figure 13 shows the speed tracking error for the nonlinear proposed controllers. It can be easily observed from this figure that IBS+SMC performs significantly better than the other three controllers.

To further quantify the difference in performance of all the applied controllers, Root Mean Square Errors (RMSE) of V_{dc} and speed tracking is given in table 6. The table clearly highlights the significant improvement of the proposed controllers over the others. The results are also supported by theoretical concepts involving these techniques. Due to integral action,

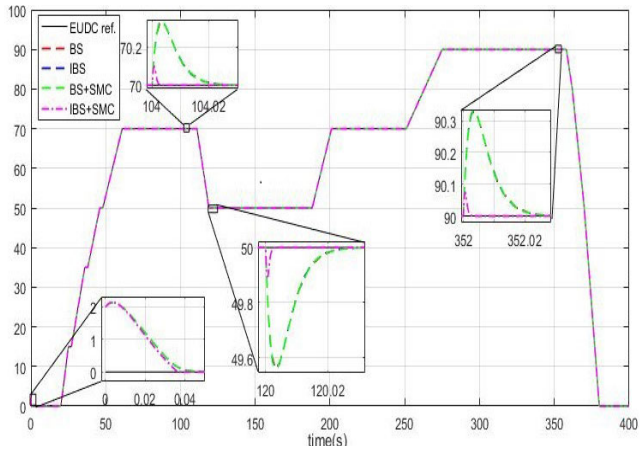

FIGURE 12. Speed tracking.

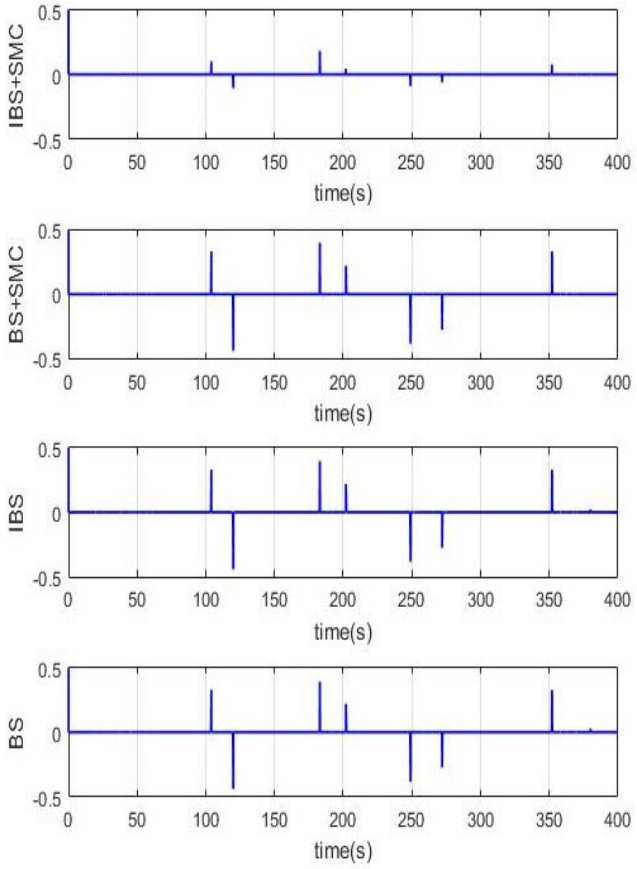

FIGURE 13. Speed error.

the steady state error of the tracking is significantly reduced; the incorporation of switching term in equation (63) gives the controller additional robustness, hence, making it better than others.

The unified model performs better voltage regulation and speed tracking than the conventional model and it is cemented by the fact that the variants of backstepping have only been applied to fuel cell control law u_1. The remaining control laws are based on normal backstepping, still there is a significant

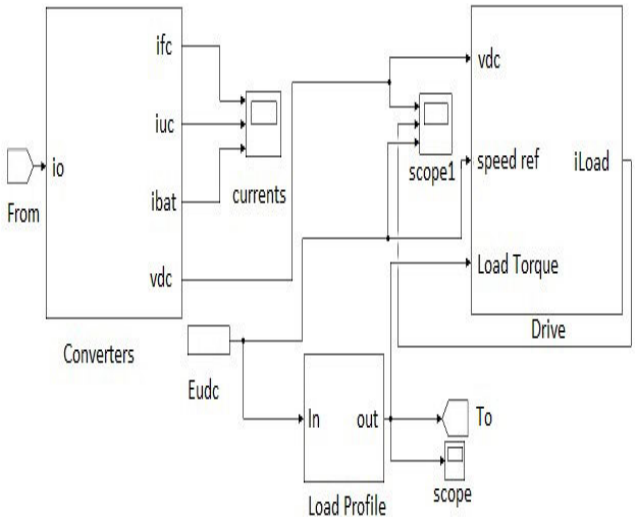

FIGURE 14. Simulation control hierarchy.

difference between the tracking of all the controllers. The effect of the different techniques in the design of FC control law u_1, for improvement of voltage regulation, has propagated to the speed tracking of the motor and vice versa. This proves irrefutably that incorporation of the motor part improves the overall performance of vehicle by improving the speed tracking and the voltage regulation. Figure 14 gives the simulation control hierarchy for simultaneous control of energy source converters and induction motor drive.

VII. CONCLUSION

In this research work, a unified model of fuel cell based hybrid electric vehicle has been proposed along with robust integral backstepping and robust backstepping controllers for DC bus voltage regulation and motor speed control. Lyapunov stability theory has been used for proving the asymptotic stability. Performance of the proposed controllers for the unified model has been analysed using MATLAB/Simulink environment. Comparative analysis of the unified model with the conventional model has been done using linear controller. The results show that unified model has significant improvements in voltage regulation and efficiently tracks the EUDC speed profile. Also, comparative analysis of nonlinear controllers with each other has been given on the unified model. The results illustrate that robust integral backstepping controller has substantially reduced the overshoots/undershoots, convergence time and steady state error; hence making robust it suitable for FHEV. Future works may encompass implementation of these control methodologies on real platforms, different energy sources and converter topologies or different controllers to further reduce speed tracking and voltage regulation errors.

REFERENCES

[1] United States Environmental Protection Agency. EPA. *Global Greenhouse Gas Emissions Data*. Accessed: Nov. 2019. [Online]. Available: https://www.epa.gov/ghgemissions/global-greenhouse-gas-emissions-data

[2] S. Shafiei and R. A. Salim, "Non-renewable and renewable energy consumption and CO_2 emissions in OECD countries: A comparative analysis," *Energy Policy*, vol. 66, pp. 547–556, Mar. 2014.
[3] B. Bilgin, P. Magne, P. Malysz, Y. Yang, V. Pantelic, M. Preindl, A. Korobkine, W. Jiang, M. Lawford, and A. Emadi, "Making the case for electrified transportation," *IEEE Trans. Transport. Electrific.*, vol. 1, no. 1, pp. 4–17, Jun. 2015.
[4] C. C. Chan, "The state of the art of electric, hybrid, and fuel cell vehicles," *Proc. IEEE*, vol. 95, no. 4, pp. 704–718, Apr. 2007.
[5] H. E. Dance, "The electric battery vehicle," *J. Inst. Electr. Eng.*, vol. 61, no. 323, pp. 1100–1108, Oct. 1923.
[6] F. A. Wyczalek, "Hybrid electric vehicles: Year 2000 status," *IEEE Aerosp. Electron. Syst. Mag.*, vol. 16, no. 3, pp. 15–25, Mar. 2001.
[7] S. Hardman, E. Shiu, and R. Steinberger-Wilckens, "Changing the fate of fuel cell vehicles: Can lessons be learnt from tesla motors?" *Int. J. Hydrogen Energy*, vol. 40, no. 4, pp. 1625–1638, Jan. 2015.
[8] Z. Dimitrova and F. Maréchal, "Techno–economic design of hybrid electric vehicles and possibilities of the multi-objective optimization structure," *Appl. Energy*, vol. 161, pp. 746–759, Jan. 2016.
[9] J. P. Torreglosa, P. Garcia, L. M. Fernandez, and F. Jurado, "Predictive control for the energy management of a fuel-cell–battery–supercapacitor tramway," *IEEE Trans Ind. Informat.*, vol. 10, no. 1, pp. 276–285, Feb. 2014.
[10] R. T. Bambang, A. S. Rohman, C. J. Dronkers, R. Ortega, and A. Sasongko, "Energy management of fuel cell/battery/supercapacitor hybrid power sources using model predictive control," *IEEE Trans Ind. Informat.*, vol. 10, no. 4, pp. 1992–2002, Nov. 2014.
[11] B. Vural, S. Dusmez, M. Uzunoglu, E. Ugur, and B. Akin, "Fuel consumption comparison of different battery/ultracapacitor hybridization topologies for fuel-cell vehicles on a test bench," *IEEE J. Emerg. Sel. Topics Power Electron.*, vol. 2, no. 3, pp. 552–561, Sep. 2014.
[12] J. Wong, N. R. N. Idris, M. Anwari, and T. Taufik, "A parallel energy-sharing control for fuel cell-battery-ultracapacitor hybrid vehicle," in *Proc. IEEE Energy Convers. Congr. Exposit.*, Sep. 2011, pp. 2923–2929.
[13] L. Guo, J. Y. Hung, and R. M. Nelms, "Evaluation of DSP-based PID and fuzzy controllers for DC–DC converters," *IEEE Trans. Ind. Electron.*, vol. 56, no. 6, pp. 2237–2248, Jun. 2009.
[14] H. K. Khalil, *Noninear System*. Upper Saddle River, NJ, USA: Prentice-Hall, 1996.
[15] N. van de Wouw, E. Lefeber, and I. L. Arteaga, *Nonlinear Systems*. Cham, Switzerland: Springer, 2017, doi: 10.1007/978-3-319-30357-4.
[16] L. Gauchia, A. Bouscayrol, J. Sanz, R. Trigui, and P. Barrade, "Fuel cell, battery and supercapacitor hybrid system for electric vehicle: Modeling and control via energetic macroscopic representation," in *Proc. IEEE Vehicle Power Propuls. Conf.*, Sep. 2011, pp. 1–6.
[17] H. Armghan, I. Ahmad, N. Ali, M. F. Munir, S. Khan, and A. Armghan, "Nonlinear controller analysis of fuel cell–battery–ultracapacitor-based hybrid energy storage systems in electric vehicles," *Arabian J. Sci. Eng.*, vol. 43, no. 6, pp. 3123–3133, Jun. 2018, doi: 10.1007/s13369-018-3137-y.
[18] D. Xu, Q. Liu, W. Yan, and W. Yang, "Adaptive terminal sliding mode control for hybrid energy storage systems of fuel cell, battery and supercapacitor," *IEEE Access*, vol. 7, pp. 29295–29303, 2019.
[19] H. El Fadil, F. Giri, J. M. Guerrero, and A. Tahri, "Modeling and nonlinear control of a fuel cell/supercapacitor hybrid energy storage system for electric vehicles," *IEEE Trans. Veh. Technol.*, vol. 63, no. 7, pp. 3011–3018, Sep. 2014.
[20] M. S. Khan, I. Ahmad, H. Armaghan, and N. Ali, "Backstepping sliding mode control of FC-UC based hybrid electric vehicle," *IEEE Access*, vol. 6, pp. 77202–77211, 2018.
[21] J. Cao and A. Emadi, "A new battery/ultracapacitor hybrid energy storage system for electric, hybrid, and plug-in hybrid electric vehicles," *IEEE Trans. Power Electron.*, vol. 27, no. 1, pp. 122–132, Jan. 2012.
[22] M. Rajabzadeh, S. M. T. Bathaee, and M. A. Golkar, "Dynamic modeling and nonlinear control of fuel cell vehicles with different hybrid power sources," *Int. J. Hydrogen Energy*, vol. 41, no. 4, pp. 3185–3198, Jan. 2016. [Online]. Available: http://www.sciencedirect.com/science/article/pii/S0360319915302056
[23] A. L. Allegre, R. Trigui, and A. Bouscayrol, "Different energy management strategies of hybrid energy storage system (HESS) using batteries and supercapacitors for vehicular applications," in *Proc. IEEE Vehicle Power Propuls. Conf.*, Sep. 2010, pp. 1–6.
[24] A. Khaligh and Z. Li, "Battery, ultracapacitor, fuel cell, and hybrid energy storage systems for electric, hybrid electric, fuel cell, and plug-in hybrid electric vehicles: State of the art," *IEEE Trans. Veh. Technol.*, vol. 59, no. 6, pp. 2806–2814, Jul. 2010.
[25] D. M. Bellur and M. K. Kazimierczuk, "DC-DC converters for electric vehicle applications," in *Proc. Electr. Insul. Conf. Electr. Manuf. Expo*, Oct. 2007, pp. 286–293.
[26] J. Hu, Y. Chen, and Z. Yang, "Study and simulation of one bi-directional dc/dc converter in hybrid electric vehicle," in *Proc. 3rd Int. Conf. Power Electron. Syst. Appl. (PESA)*, May 2009, pp. 1–4.
[27] R. Kumari and P. R. Thakura, "Development of fly back converter for hybrid electric vehicles," in *Proc. Int. Conf. Power, Energy Control (ICPEC)*, Feb. 2013, pp. 335–340.
[28] O. Hegazy, J. V. Mierlo, and P. Lataire, "Analysis, modeling, and implementation of a multidevice interleaved DC/DC converter for fuel cell hybrid electric vehicles," *IEEE Trans. Power Electron.*, vol. 27, no. 11, pp. 4445–4458, Nov. 2012.
[29] A. Nahavandi, M. T. Hagh, M. B. B. Sharifian, and S. Danyali, "A non-isolated multiinput multioutput DC–DC boost converter for electric vehicle applications," *IEEE Trans. Power Electron.*, vol. 30, no. 4, pp. 1818–1835, Apr. 2015.
[30] M. S. Khan, I. Ahmad, and F. Z. Ul Abideen, "Output voltage regulation of FC-UC based hybrid electric vehicle using integral backstepping control," *IEEE Access*, vol. 7, pp. 65693–65702, 2019.
[31] T. Hua, R. Ahluwalia, L. Eudy, G. Singer, B. Jermer, N. Asselin-Miller, S. Wessel, T. Patterson, and J. Marcinkoski, "Status of hydrogen fuel cell electric buses worldwide," *J. Power Sour.*, vol. 269, pp. 975–993, Dec. 2014.
[32] V. Das, S. Padmanaban, K. Venkitusamy, R. Selvamuthukumaran, F. Blaabjerg, and P. Siano, "Recent advances and challenges of fuel cell based power system architectures and control—A review," *Renew. Sustain. Energy Rev.*, vol. 73, pp. 10–18, Jun. 2017.
[33] O. Z. Sharaf and M. F. Orhan, "An overview of fuel cell technology: Fundamentals and applications," *Renew. Sustain. Energy Rev.*, vol. 32, pp. 810–853, Apr. 2014.
[34] H.-W. Wu, "A review of recent development: Transport and performance modeling of PEM fuel cells," *Appl. Energy*, vol. 165, pp. 81–106, Mar. 2016.
[35] M. A. Hannan, M. M. Hoque, A. Mohamed, and A. Ayob, "Review of energy storage systems for electric vehicle applications: Issues and challenges," *Renew. Sustain. Energy Rev.*, vol. 69, pp. 771–789, Mar. 2017.
[36] U. R. Prasanna, P. Xuewei, A. K. Rathore, and K. Rajashekara, "Propulsion system architecture and power conditioning topologies for fuel cell vehicles," *IEEE Trans. Ind. Appl.*, vol. 51, no. 1, pp. 640–650, Jan. 2015.
[37] L. Andaloro, A. Arista, G. Agnello, G. Napoli, F. Sergi, and V. Antonucci, "Study and design of a hybrid electric vehicle (Lithium batteries-PEM FC)," *Int. J. Hydrogen Energy*, vol. 42, no. 5, pp. 3166–3184, Feb. 2017.
[38] Z. Mokrani, D. Rekioua, and T. Rekioua, "Modeling, control and power management of hybrid photovoltaic fuel cells with battery bank supplying electric vehicle," *Int. J. Hydrogen Energy*, vol. 39, no. 27, pp. 15178–15187, Sep. 2014.
[39] Z. Zou, J. Cao, B. Cao, and W. Chen, "Evaluation strategy of regenerative braking energy for supercapacitor vehicle," *ISA Trans.*, vol. 55, pp. 234–240, Mar. 2015.
[40] J. M. Blanes, R. Gutiérrez, A. Garrigós, J. L. Lizán, and J. M. Cuadrado, "Electric vehicle battery life extension using ultracapacitors and an FPGA controlled interleaved buck–boost converter," *IEEE Trans. Power Electron.*, vol. 28, no. 12, pp. 5940–5948, Dec. 2013.
[41] J. Y. Yong, V. K. Ramachandaramurthy, K. M. Tan, and N. Mithulananthan, "A review on the state-of-the-art technologies of electric vehicle, its impacts and prospects," *Renew. Sustain. Energy Rev.*, vol. 49, pp. 365–385, Sep. 2015.
[42] H. Zhao, B. Gao, B. Ren, and H. Chen, "Integrated control of in-wheel motor electric vehicles using a triple-step nonlinear method," *J. Franklin Inst.*, vol. 352, no. 2, pp. 519–540, Feb. 2015.
[43] L. Kumar and S. Jain, "Electric propulsion system for electric vehicular technology: A review," *Renew. Sustain. Energy Rev.*, vol. 29, pp. 924–940, Jan. 2014.
[44] A. Raisemche, M. Boukhnifer, C. Larouci, and D. Diallo, "Two active fault-tolerant control schemes of induction-motor drive in EV or HEV," *IEEE Trans. Veh. Technol.*, vol. 63, no. 1, pp. 19–29, Jan. 2014.
[45] D. Traoré, J. De Leon, and A. Glumineau, "Adaptive interconnected observer-based backstepping control design for sensorless induction motor," *Automatica*, vol. 48, no. 4, pp. 682–687, Apr. 2012.

SYED AHMAD SIFFAT received the B.S. degree from COMSATS University Islamabad, Lahore, Pakistan, in 2018. He is currently pursuing the M.S. degree in electrical engineering with specialization in power and control system at the School of Electrical Engineering and Computer Science, National University of Sciences and Technology (NUST), Islamabad, Pakistan.

IFTIKHAR AHMAD received the M.S. degree in fluid mechanical engineering from University of Paris VI (University Pierre and Marie Curie), Paris, and the Ph.D. degree in robotics, control, and automation from the Universite de Versailles, France.

He is currently an Assistant Professor with the Department of Electrical Engineering, School of Electrical Engineering and Computer Science, NUST, Islamabad, Pakistan. His main research interests include nonlinear systems, robotics, automation and control, hybrid electrical vehicles, and maximum power point tracking.

AQEEL UR RAHMAN received the B.S. degree from the Mirpur University of Science and Technology, in 2017, and the M.S. degree in electrical engineering with specialization in power and control system from the School of Electrical Engineering and Computer Science, National University of Sciences and Technology (NUST), Islamabad, Pakistan, in 2019.

YASIR ISLAM received the B.S. and M.S. degrees in electrical engineering with specialization in power and control system from the School of Electrical Engineering and Computer Science, National University of Sciences and Technology (NUST), Islamabad, Pakistan.